analytical chemistry

Letter

Cite This: Anal. Chem. 2019, 91, 10357−10360

pubs.acs.org/ac

Single Chain Cationic Polymer Dot as a Fluorescent Probe for Cell Imaging and Selective Determination of Hepatocellular Carcinoma Cells

Sezer Özenler,[†,⊥] Muge Yucel,[‡,⊥] Özge Tüncel,[†] Hakan Kaya,[‡] Serdar Özçelik,[*,†,§,∥] and Umit Hakan Yildiz[*,†,§]

[†]Department of Chemistry, Izmir Institute of Technology, Urla 35430, Izmir, Turkey

[‡]Department of Bioengineering, Izmir Institute of Technology, Urla 35430, Izmir, Turkey

[§]Department of Photonics, Izmir Institute of Technology, Urla 35430, Izmir, Turkey

[∥]Department of Radiation Oncology, School of Medicine, Stanford University, Palo Alto, California 94305, United States

Supporting Information

ABSTRACT: This letter describes formation of single chain cationic polymer dots (Pdots) made of poly[1,4-dimethyl-1-(3-((2,4,5-trimethylthiophen-3-yl)oxy)propyl)piperazin-1-ium bromide] conjugated polyelectrolyte (CPE). The single chain Pdot formation relies on a simple process which is a rapid nanophase separation between CPE solution of ethylene glycol and water. Pdots show narrow monodisperse size distribution with a 3.6 nm in diameter exhibiting high brightness and excellent colloidal and optical stability. It has been demonstrated that photoluminescent Pdots provide selective nuclear translocation to hepatocellular carcinoma cells as compared to healthy liver cells. The Pdot labeling effectively discriminates cancer cells in the coculture media. Pdots hold great promise as a luminescent probe to diagnose cancer cells in histology and may guide surgeons during operations to precisely separate out cancerous tissue due to augmented fluorescence brightness.

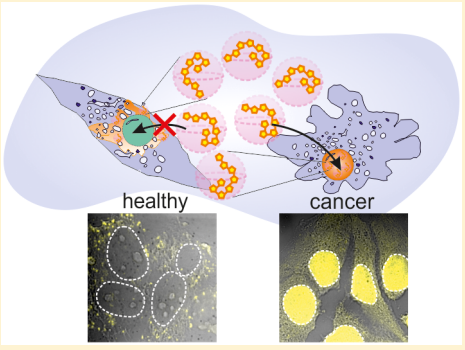

Recent efforts devoted to develop fluorescent soft nanoparticles have profoundly revolutionized routines in bioimaging,[1−6] diagnostics,[7,8] and drug therapy studies.[9] In addition to their excellent emissive properties,[4] chemical modularity, and biocompatibility,[10] soft nanoparticles exhibit reversible deformations and chain displacement by the conformational alteration of their polymer backbone, causing significant changes in photophysical properties.[11,12] By this unique property, soft nanoparticles show extraordinary penetration capability both in inter- and intracellular milieu. The recent reports about conjugated polymer nanoparticles (CPNs) and polymer dots (Pdots) have exemplified a number of attracting applications such as in vitro and in vivo imaging and diagnosis.[3,13] Unlike CPNs with larger diameters of >30 nm, single chain Pdots in reduced diameter (<10 nm) have shown greater an extinction coefficient, higher photoluminescence quantum yield, brightness, photostability, and colloidal stability.[13−15] Therefore, in biological applications, single chain Pdots are expected to show unambiguous advantages over CPNs; for instance, single chain Pdots with diameters <10 nm can access crowded and restricted subcellular space and are found to be more efficient for labeling subcellular features[16,17] as well as cellular biomarkers.[18] However, preparation of single chain Pdots by established protocols such as nanoprecipitation is a bottleneck and often not applicable as it may cause coprecipitation of multiple polymer chains. Modified nanoprecipitation,[6,19] two-step reprecipitation,[16,20] and utilization of solid support[21] for obtaining single chain Pdots were suggested as alternative methodologies to overcome the coprecipitation problem. Herein, a nanophase separation method is proposed to prepare a single chain Pdot with a size of 3.6 nm without using any solid support. The Pdots are formed by rapid nanophase separation occurring between water (a poor solvent) and ethylene glycol (a good solvent) that contains a cationic single chain of poly[1,4-dimethyl-1-(3-((2,4,5-trimethylthiophen-3-yl)oxy)propyl)piperazin-1-ium bromide]. The smaller Pdots provide substantial advantages for penetration into cellular compartments having pore size between 5 and 10 nm.[22−25] This argument has been confirmed by applying Pdots to the hepatocellular carcinoma and healthy liver cells which shows that our Pdots exhibit selective determination of hepatocellular carcinoma (HCC) cells. The extremely small sized Pdots showing extensive labeling of cancer cells in coculture medium have a great potential for discriminating the cancer cells in healthy tissues. Therefore, this property facilitates a fast translation of Pdots to the clinical

Received: May 17, 2019
Accepted: July 23, 2019
Published: July 23, 2019

Downloaded via IZMIR YUKSEK TEKNOLOJI ENSTITUSU on October 24, 2022 at 13:12:05 (UTC).
See https://pubs.acs.org/sharingguidelines for options on how to legitimately share published articles.

© 2019 American Chemical Society

DOI: 10.1021/acs.analchem.9b02300
Anal. Chem. 2019, 91, 10357−10360

practice for pinpointing the tumor microenvironment and surgical borders.

Scheme 1 illustrates the formation process of Pdots containing a single conjugated polyelectrolyte (CPE) chain driven by rapid nanophase separation between the ethylene glycol (good solvent) and water (poor solvent) (see video in the Supporting Information for dissolution of CPE in ethylene glycol and water). More explicitly, CPE−ethylene glycol interaction is entropically more favorable than the CPE−water interaction, which induces nanophase separation of CPE-rich ethylene glycol phase. Overall, a single CPE chain enveloped in ethylene glycol as a Pdot and its random coil conformation helps keep colloidal stability in the water. The structure of CPEs used in this work is shown in Figure 1a, confirmed by NMR (Figures S2, S4, and S7, Supporting Information). Atomic force microscopy (AFM) imaging of Pdots deposited on a mica surface was conducted which showed monodispersed objects, as shown in Figure 1b. The average height distribution determined by AFM given in Figure 1c was found to be 1 nm, which is consistent with a single chain dimension of CPE. Based on theoretical calculations, the radius gyration (Rg) was found to be 2.2 nm, corresponding to

Scheme 1. Schematic Illustration of Nanophase Separation between Ethylene Glycol (EG) and Water during Pdot Formation

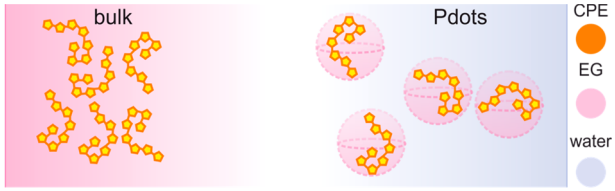

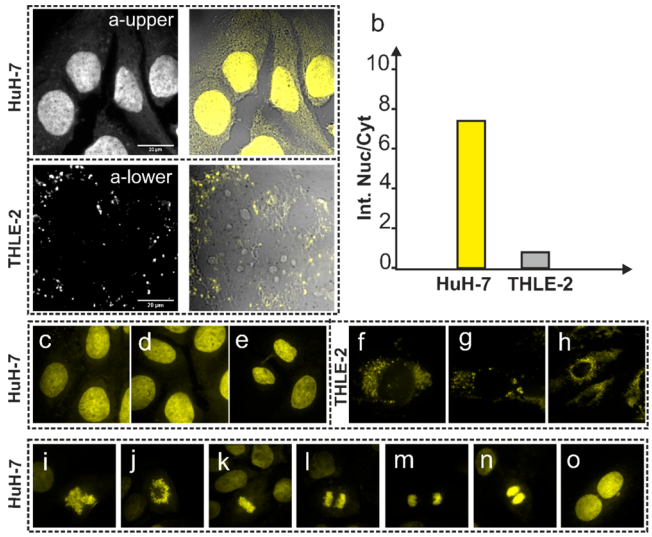

Figure 2. (a) Bright field and fluorescent images of a-upper: HuH-7 and a-lower: THLE-2 cells. (b) Fluorescence intensity ratio of nucleus to cytoplasm (intensity analysis has performed by ImageJ from the images shown in Figure 2a). (c−h) Concentration dependent study of the Pdots by increasing from 40 to 100 μM. (i−o) The compartmentalization of Pdots in the nuclei demonstrated with phases of mitotic divisions in the cell cycle. Images were arranged to represent phases starting from (i) prophase, (j) pro-metaphase, (k) metaphase, (l) anaphase, (m) telophase, (n) cytokinesis, and (o) newly divided cells.

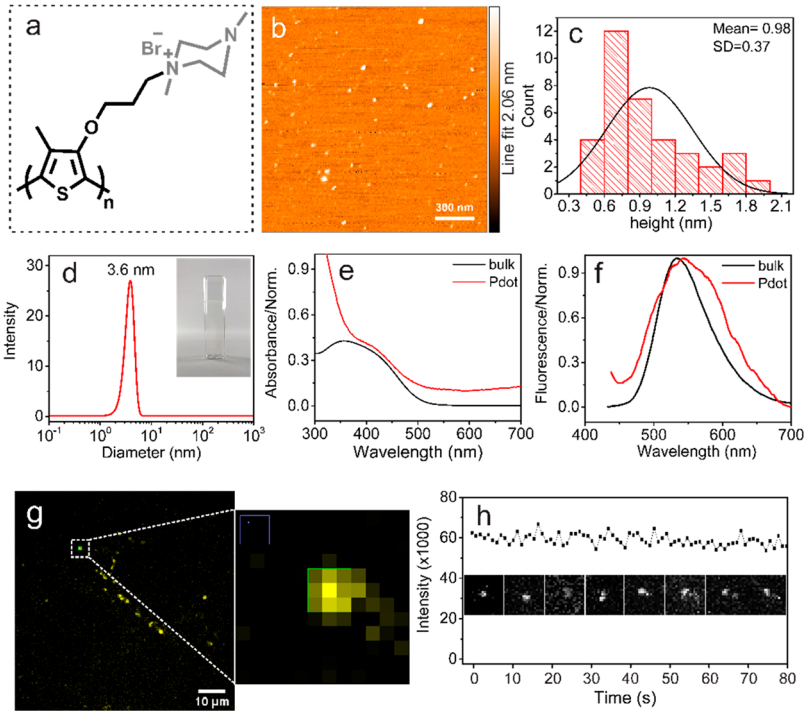

Figure 1. (a) Chemical structure of cationic conjugated polymer. (b) AFM image of Pdots. (c) Histogram of a height distribution of Pdots measured by AFM. (d) Hydrodynamic diameter distribution of Pdots by DLS (inset photograph shows 1.6 mg/L Pdot solution). (e) Absorption spectra of bulk and Pdot solutions. (f) Fluorescence spectra of bulk and Pdot solutions. (g) Confocal micrograph of Pdots in culture medium (inset image is the 100× magnification of the selected Pdot). (h) Fluorescence intensity variation of a single Pdot over 80 s.

DOI: 10.1021/acs.analchem.9b02300
Anal. Chem. 2019, 91, 10357−10360

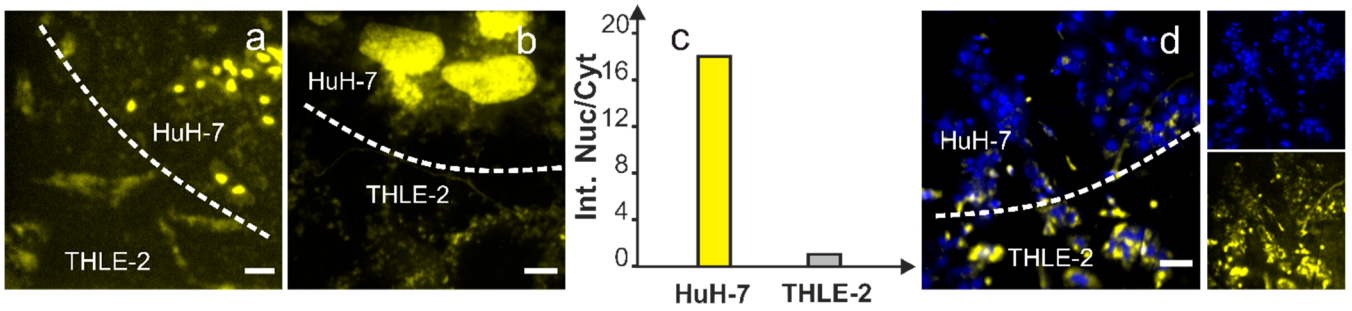

Figure 3. Images of cocultured THLE-2 and HuH-7 cells (a) 20× magnification (scale bar: 50 μm) and (b) 100× magnification (scale bar: 10 μm). THLE-2 cells (1×10^4 cell/well) were seeded on glass bottom plates. After 1 day, the culture medium was discarded; HuH-7 cells were plated at a density of 1×10^4 cell/well, and the cells were allowed to grow together. The cells were treated with Pdots for 24 h and then fixed. (c) fluorescence intensity ratio of nucleus to cytoplasm (intensity analysis has performed by ImageJ from the images shown in Figure 3a). (d) The images that were captured after DAPI and Pdot staining were merged (scale bar: 50 μm). Blue colored nuclei were DAPI stained cells. Yellow colored spots were Pdots accumulated in the cells (inset figures showing DAPI only (upper) and Pdot only (lower)).

20 mers (Figure S8, Supporting Information), which is the dimension of single CPE chain. Dynamic light scattering (DLS) results revealed that the Pdots have a diffusion coefficient of 4.17 $\mu m^2/s$, which refers to 3.6 nm in diameter, as shown in Figure 1d. DLS yielded a slightly larger particle size than AFM due to the contribution of solvent molecules to the hydrodynamic radius of polymer; nevertheless, particle sizes determined by the two methods are consistent with each other.[6] Figure 1e shows absorption spectra of both bulk CPE and Pdots. There are two major peaks at 365 and 415 nm in the bulk spectrum, corresponding to $\pi-\pi^*$ transitions of shorter and longer conjugation length species. In contrast, Pdot spectrum exhibits a single feature at 415 nm, which may refer to the existence of nearly identical backbone conformation of single polymer chain. Figure 1f illustrates the fluorescence spectra of bulk CPE and Pdots showing maxima at 540 and 550 nm, respectively. The Pdot spectral maximum exhibits 10 nm red-shift as compared to the bulk as well as a shoulder at 570 nm, attributable to elongation of conjugation length or increased intrachain $\pi-\pi$ interactions. Figure 1g shows the confocal microscope image of Pdots upon excitation at 488 nm in cell culture medium, which shows that the Pdots retained their shape and integrity. The inset figure shows the fluorescence spot of a single Pdot, which has bright and dimmer intensity at the center and peripheral pixels, respectively. These results reveal that individual Pdots exhibit detectable fluorescence intensity and preserve colloidal and optical stability without coalescence and quenching in the cell culture medium. Figure 1h illustrates the fluorescence intensity variation of a selected single Pdot shown in the inset images (488 nm, 1 mW of power at the sample and 700 ms of illumination time) for 80 s. The Pdot exhibits 5.3×10^4 (std. dev. = 2.7×10^3) mean fluorescence intensity over the observation period (from a minute to hours). Further analysis of many spots representing Pdots was performed, and no diminishing intensity was observed (Figure S9, Supporting Information). These results ascertaining the Pdots have remarkable photostability under continuous illumination and may serve as a probe for single particle tracking experiments in cell culture medium. The facile preparation protocol of Pdots and their colloidal and fluorescence stability make them a superior probe for cell imaging applications. Moreover, monodispersed Pdots with small size show penetration ability to the subcellular compartments.

As a demonstrative example, we employed Pdots as a subcellular imaging probe. Hepatocellular carcinoma (HuH-7 cells) and healthy adult liver epithelial cells (THLE-2 cells) were used to assess accumulation of Pdots in the cells. Figure 2a (upper panel) shows HuH-7 cells where Pdots were localized in the nuclei, whereas they accumulated in cytoplasm and around the nuclei of THLE-2 cells (Figure 2a, lower panel). The fluorescence intensity ratio of nucleus to cytoplasm is given in Figure 2b, indicating that HuH-7 cells exhibit a sevenfold greater intensity ratio as compared to that of the THLE-2 cells. These results show that the accumulation profile of Pdots in the subcellular region is significantly dependent on the cell type. Pdots were mostly and selectively compartmentalized in the nuclei of HuH-7 cells. We conducted a concentration dependent study of the Pdots by varying the concentration from 40 to 100 μM, as shown in Figure 2c–h, for both HuH-7 and THLE-2 cells. Pdots were mostly located in the nuclei for HuH-7, whereas they dispersed in the cytoplasm and accumulated around the nuclei for THLE-2 independent from their initial concentration. The size of nuclear pore complexes was reported to be about 5–10 nm, allowing free diffusion of the yellow emitting Pdots (Figure S10, Supporting Information, for Pdot trajectories indicating confined and directed type of diffusions). As reported earlier, the nuclear pore complex (NPC) mediates trafficking between the cytoplasm and nucleoplasm, and overexpression of several associated nuclear export factors has been linked to cancers.[24,25] Therefore, selective nuclear translocation of Pdots is attributed to the relatively larger size of the nuclear pores and altered nuclear membrane structure of HuH-7 as compared to THLE-2.

Beyond their selective translocation, Pdots exhibited high resolution for nuclei chromosomal staining, which occurred due to electrostatic interaction between nuclear DNA and cationic characteristics of Pdots. As shown in Figure 2i–o, we demonstrated mitotic division phases of HuH-7 cells. The phases of interphase, metaphase, anaphase, and telophase were easily recognized for the HuH-7 cells. These findings prove that the Pdots can be notably used as chromosome or nuclei probes as well.

The benefit of selective translocation of Pdots into the nuclei of cancer cells is clear and holds promise for effortless discrimination of hepatocarcinoma and healthy liver cells. To prove this postulate, we conducted a coculture experiment for HuH-7 and THLE-2 cells. Figure 3a, b shows the coculture

DOI: 10.1021/acs.analchem.9b02300
Anal. Chem. 2019, 91, 10357–10360

image of HuH-7 and THLE-2 cells, revealing that the Pdots were located in the nuclei of the HuH-7; on the contrary, they were in the cytoplasm and mostly located around the nuclei of THLE-2 cells. Pdots show two different fluorescence intensity distribution profiles where the maxima are centered around 1.8×10^6 and 1.0×10^5, as observed in Figure 3c. The higher intensity was collected from nuclei of HuH-7 cells, whereas lower intensity was from the nuclei of the THLE-2 cells, indicating that Pdots accumulated 18-fold greater in HuH-7 nuclei as compared to THLE-2 nuclei. This finding proves that Pdots are capable of selective labeling of HCC in a coculture environment as an analogy of the tumor microenvironment and simplifies determination of borders at the cellular level (the dotted white line was intentionally drawn to indicate the border between healthy and cancerous regions). Furthermore, DAPI staining which labels both the nuclei indiscriminatingly was used to monitor the nuclei of HuH-7 and THLE-2 cells. The cell population above the dotted line in Figure 3d refers to HuH-7 cancer cells where the DAPI and Pdot staining overlapped. On the other hand, below the dotted line, both DAPI and Pdot costaining was observed in the nuclei and cytoplasm, respectively. It can be concluded that Pdots stain selectively the nuclei of the HuH-7 cells and the cytoplasm of the THLE-2 cells.

Overall, Pdots are potential probes for selective nuclear labeling that discriminate HCC cells over healthy liver cells in the coculture media as well as in the tumor microenvironment. Moreover, this attractive potential of Pdots may find effortless translation for precisely determining surgical borders in cancerous tissues, discriminating cell histological examinations.

■ ASSOCIATED CONTENT

Supporting Information

The Supporting Information is available free of charge on the ACS Publications website at DOI: 10.1021/acs.analchem.9b02300.

Experimental section, NMR and mass spectra, and theoretical details (PDF)

Video of dissolution of CPE in ethylene glycol and water (MPG

■ AUTHOR INFORMATION

Corresponding Authors

*E-mail: hakanyildiz@iyte.edu.tr; Fax: +90 232 750 7509.

*E-mail: ozcelik@stanford.edu or serdarozcelik@iyte.edu.tr.

ORCID

Sezer Özenler: 0000-0001-6045-7035

Muge Yucel: 0000-0001-7032-392X

Özge Tüncel: 0000-0002-0873-133X

Hakan Kaya: 0000-0001-9739-9676

Serdar Özçelik: 0000-0003-2029-0108

Umit Hakan Yildiz: 0000-0002-6922-4454

Author Contributions

⊥S.Ö. and M.Y. contributed equally.

Notes

The authors declare no competing financial interest.

■ ACKNOWLEDGMENTS

This work was supported by the The Scientific and Technological Research Council of Turkey, TUBİTAK Project 116Z547 with partial support by TUBİTAK Project 116Z337.Authors S.Ö. and M.Y. are YÖK 100-2000 scholarship holders.

■ REFERENCES

(1) Wu, C.; Schneider, T.; Zeigler, M.; Yu, J.; Schiro, P. G.; Burnham, D. R.; McNeill, J. D.; Chiu, D. T. *J. Am. Chem. Soc.* **2010**, *132* (43), 15410−15417.

(2) Yu, J.; Rong, Y.; Kuo, C.-T.; Zhou, X.-H.; Chiu, D. T. *Anal. Chem.* **2017**, *89* (1), 42−56.

(3) Yang, Y.; Chen, J.; Yang, Y.; Xie, Z.; Song, L.; Zhang, P.; Liu, C.; Liu, J. *Nanoscale* **2019**, *11*, 7754.

(4) Kuo, C.-T.; Thompson, A. M.; Gallina, M. E.; Ye, F.; Johnson, E. S.; Sun, W.; Zhao, M.; Yu, J.; Wu, I. C.; Fujimoto, B.; DuFort, C. C.; Carlson, M. A.; Hingorani, S. R.; Paguirigan, A. L.; Radich, J. P.; Chiu, D. T., Optical painting and fluorescence activated sorting of single adherent cells labelled with photoswitchable Pdots. *Nat. Commun.* **2016**, *7* (1). DOI: 10.1038/ncomms11468

(5) Wu, C.; Bull, B.; Szymanski, C.; Christensen, K.; McNeill, J. *ACS Nano* **2008**, *2* (11), 2415−2423.

(6) Pu, K.; Mei, J.; Jokerst, J. V.; Hong, G.; Antaris, A. L.; Chattopadhyay, N.; Shuhendler, A. J.; Kurosawa, T.; Zhou, Y.; Gambhir, S. S.; Bao, Z.; Rao, J. *Adv. Mater.* **2015**, *27* (35), 5184−5190.

(7) Moon, J. H.; MacLean, P.; McDaniel, W.; Hancock, L. F. *Chem. Commun.* **2007**, No. 46, 4910−4912.

(8) Sun, K.; Tang, Y.; Li, Q.; Yin, S.; Qin, W.; Yu, J.; Chiu, D. T.; Liu, Y.; Yuan, Z.; Zhang, X.; Wu, C. *ACS Nano* **2016**, *10* (7), 6769−6781.

(9) Ding, D.; Pu, K.-Y.; Li, K.; Liu, B. *Chem. Commun.* **2011**, *47* (35), 9837.

(10) Guo, B.; Sheng, Z.; Kenry, K.; Hu, D.; Lin, X.; Xu, S.; Liu, C.; Zheng, H.; Liu, B. *Mater. Horiz.* **2017**, *4* (6), 1151−1156.

(11) Hu, D.; Yu, J.; Padmanaban, G.; Ramakrishnan, S.; Barbara, P. F. *Nano Lett.* **2002**, *2* (10), 1121−1124.

(12) Eder, T.; Stangl, T.; Gmelch, M.; Remmerssen, K.; Laux, D.; Höger, S.; Lupton, J. M.; Vogelsang, J., Switching between H- and J-type electronic coupling in single conjugated polymer aggregates. *Nat. Commun.* **2017**, *8* (1). DOI: 10.1038/s41467-017-01773-0

(13) Feng, L.; Zhu, C.; Yuan, H.; Liu, L.; Lv, F.; Wang, S. *Chem. Soc. Rev.* **2013**, *42* (16), 6620.

(14) Tuncel, D.; Demir, H. V. *Nanoscale* **2010**, *2* (4), 484.

(15) Grey, J. K.; Kim, D. Y.; Norris, B. C.; Miller, W. L.; Barbara, P. F. *J. Phys. Chem. B* **2006**, *110* (51), 25568−25572.

(16) Sun, K.; Chen, H.; Wang, L.; Yin, S.; Wang, H.; Xu, G.; Chen, D.; Zhang, X.; Wu, C.; Qin, W. *ACS Appl. Mater. Interfaces* **2014**, *6* (13), 10802−10812.

(17) Yu, J.; Wu, C.; Zhang, X.; Ye, F.; Gallina, M. E.; Rong, Y.; Wu, I.-C.; Sun, W.; Chan, Y.-H.; Chiu, D. T. *Adv. Mater.* **2012**, *24* (26), 3498−3504.

(18) Wu, L.; Wu, I. C.; DuFort, C. C.; Carlson, M. A.; Wu, X.; Chen, L.; Kuo, C.-T.; Qin, Y.; Yu, J.; Hingorani, S. R.; Chiu, D. T. *J. Am. Chem. Soc.* **2017**, *139* (20), 6911−6918.

(19) Ye, F.; Wu, C.; Jin, Y.; Wang, M.; Chan, Y.-H.; Yu, J.; Sun, W.; Hayden, S.; Chiu, D. T. *Chem. Commun.* **2012**, *48* (12), 1778−1780.

(20) Wu, C.; Szymanski, C.; McNeill, J. *Langmuir* **2006**, *22* (7), 2956−2960.

(21) Ye, F.; Sun, W.; Zhang, Y.; Wu, C.; Zhang, X.; Yu, J.; Rong, Y.; Zhang, M.; Chiu, D. T. *Langmuir* **2015**, *31* (1), 499−505.

(22) Simon, D. N.; Rout, M. P. Cancer and the Nuclear Pore Complex. In *Cancer Biology and the Nuclear Envelope: Recent Advances May Elucidate Past Paradoxes*; Schirmer, E. C., de las Heras, J. I., Eds.; Springer New York: New York, NY, 2014; pp 285−307.

(23) Pu, K.-Y.; Li, K.; Liu, B. *Adv. Mater.* **2010**, *22* (5), 643−646.

(24) Paine, P. L.; Moore, L. C.; Horowitz, S. B. *Nature* **1975**, *254* (5496), 109−114.

(25) Sakuma, S.; D'Angelo, M. A. *Semin. Cell Dev. Biol.* **2017**, *68*, 72.

DOI: 10.1021/acs.analchem.9b02300
Anal. Chem. 2019, 91, 10357−10360